

Energy-Dependent LDOS Modulation in Cuprate Superconductors

Degang Zhang and C. S. Ting

Texas Center for Superconductivity and Department of Physics, University of Houston, Houston, TX 77204, USA

Motivated by the recent scanning tunneling microscopy (STM) experiment [J. E. Hoffman, et al., *Science* 297, 1148 (2002)], we investigate the energy-dependent modulation induced by a weak and extended defect in a d-wave superconductor. The Fourier component of the local density of states (LDOS) is calculated up to the first order in the defect parameters. Our numerically obtained images match together with the energy-dependent charge modulation wave vectors at different dopings exhibit the essential features as those measured by the experiment. We also predict new modulation wave vectors in the first Brillouin zone. Hopefully, they could be verified by future STM experiments.

PACS number(s): 74.25.-q, 74.72.-h, 74.62.Dh

In the past year, a series of scanning tunneling spectroscopy (STM) experiments have confirmed the coexistence of charge modulation and superconductivity in $\text{Bi}_2\text{Sr}_2\text{CaCu}_2\text{O}_{8+x}$ [1, 2, 3]. In a magnetic field, Hoffman et al. [1] discovered a four-cell checkerboard local density of states (LDOS) modulation localized in a small region around the vortex core. The field-induced charge modulation oriented parallel to the $\text{Cu}-\text{O}$ bond directions is relatively strong. Subsequently, Howard et al. [2] also observed similar checkerboard charge modulation in absence of magnetic field for a wide range of bias voltages, but with relatively weak intensity.

Recently Hoffman et al. [3] investigated the zero-field charge modulation by employing high resolution Fourier transform scanning tunneling spectroscopy. They found that the period of the charge modulation depends on the energy and doping for the bias voltages below the maximum superconducting gap. With the bias voltage (doping level) or doping (bias voltage level) increasing, the LDOS modulation wave vectors oriented parallel to the $(\pi; 0)$ and $(0; \pi)$ directions become shorter while those oriented parallel to the $(\pi; \pi)$ directions become longer.

A number of theoretical studies on the STM spectra have already been carried out by several authors [4-7] in attempt to explain the zero-field LDOS modulation observed by Howard et al. [2]. There are also works [8-10] trying to understand the energy-dependent LDOS modulation observed in the zero-field STM experiment [3]. In Ref. [8], Wang and Lee proposed that the experimental observation of Hoffman et al. [3] is a result of the quasiparticle interference induced by an impurity with an on-site potential of moderate strength. However, these calculations [8-10] seem only able to address a limited portion of the STM experimental measurements [3], and do not give the relations among the peaks associated with the modulation wave vectors, dopings and the bias voltages as those presented in Ref. [3].

In this paper, we examine the effects of the scattering of a quasiparticle by a weak and extended defect or im-

purity with both hopping and pairing disorders on the Fourier transform of the LDOS. Using the first order T-matrix approximation, we show that our results are consistent with all the essential features observed in the experiment of Ref. [3]. In addition, we predict new modulation wave vectors existed in the first Brillouin zone, hopefully they could be verified by future STM experiments.

The Hamiltonian describing the scattering of quasiparticles from a single defect with local modulations of both hopping and pairing parameters in a d-wave superconductor can be written as

$$\begin{aligned}
 H &= H_{\text{BCS}} + H_{\text{imp}}; \\
 H_{\text{BCS}} &= \sum_{\mathbf{k}} (\epsilon_{\mathbf{k}} - \mu) c_{\mathbf{k}}^\dagger c_{\mathbf{k}} + \sum_{\mathbf{k}} \epsilon_{\mathbf{k}} (c_{\mathbf{k}}^\dagger c_{-\mathbf{k}}^\dagger + c_{-\mathbf{k}} c_{\mathbf{k}}); \\
 H_{\text{imp}} &= \sum_{\langle ij \rangle} t_{ij} c_i^\dagger c_j + \sum_{\langle ij \rangle} \Delta_{ij} (c_i^\dagger c_{j\#}^\dagger + c_{j\#} c_i) \\
 &\quad + (V_s + V_m) c_0^\dagger c_0 + (V_s - V_m) c_{0\#}^\dagger c_{0\#}; \quad (1)
 \end{aligned}$$

Here μ is the chemical potential to be determined by doping, $\epsilon_{\mathbf{k}} = t_1(\cos k_x + \cos k_y) + t_2 \cos k_x \cos k_y + t_3(\cos 2k_x + \cos 2k_y) + t_4(\cos 2k_x \cos k_y + \cos k_x \cos 2k_y) + t_5 \cos 2k_x \cos 2k_y$, where $t_{1-5} = 0.5951; 0.1636; 0.0519; 0.1117; 0.0510$ (eV). The band parameters are taken from those of Norman et al. [11] for $\text{Bi}_2\text{Sr}_2\text{CaCu}_2\text{O}_{8+x}$, and the lattice constant a is set as $a = 1$. The order parameter away from the impurity is given by $\Delta_{\mathbf{k}} = \Delta_0(\cos k_x - \cos k_y)$.

Without loss of generality, at the impurity or defect site, we assume an on-site potential consisting of a non-magnetic part, V_s , and a magnetic part, V_m . The defect also induces a weak local modulation in the hopping, t , to the nearest neighbor sites, and a suppression of the superconductivity order parameter on the four bonds connected to the impurity site, c_1 , and on the other twelve bonds connected to the nearest neighbor sites, c_2 .

The Hamiltonian (1) has in fact been successfully applied by Tang and Flatté [12] to explain the resonant STM spectra for Ni impurities in $\text{Bi}_2\text{Sr}_2\text{CaCu}_2\text{O}_{8+x}$. In the present situation, no resonances in LDOS have been observed in the recent STM experiments [2, 3]. So it is reasonable to assume that the on-site potentials (V_s and V_m) and the modifications in hopping and pairing parameters (t_1 , t_2 and Δ) are all weak and have approximately the same order of magnitude. In order to compare with the measurements in the STM experiment [3], we investigate three different hole doping cases: underdoping (10 percent) with $\mu_0 = 50$ meV, optimally doped (15 percent) with $\mu_0 = 44$ meV, and overdoping (17 percent) with $\mu_0 = 37$ meV. Here we shall not discuss the issue as to why the underdoped case has a higher μ_0 value, and simply accept it as an experimental fact [3].

Our method to solve the Hamiltonian (1) and to obtain the LDOS is the standard Bogoliubov transformation plus Green's function technique. When t_1 , t_2 , V_s and V_m are all small, keeping the leading term in the T-matrix approach should be good approximation. The Fourier component of the LDOS obtained in such an approximation can be shown to have the following form

$$g_k(\omega) = \frac{2}{N} \sum_{\mathbf{k}} \sum_{\mathbf{q}} \text{Im} [G_k^0(\omega) G_{\mathbf{k}+\mathbf{q}}^0(\omega)] \frac{1}{\omega - E_{\mathbf{k}} + i0^+} + 2[t_1 B(\mathbf{k}; \mathbf{q}) + t_2 C(\mathbf{k}; \mathbf{q})] \frac{1}{\omega - E_{\mathbf{k}} + i0^+} g_{\mathbf{k}+\mathbf{q}}(\omega) \quad (2)$$

where N is the number of sites in the lattice, $A(\mathbf{k}; \mathbf{q}) = \cos k_x + \cos k_y + \cos(k_x + q_x) + \cos(k_y + q_y)$, $B(\mathbf{k}; \mathbf{q}) = \cos k_x - \cos k_y + \cos(k_x + q_x) - \cos(k_y + q_y)$, $C(\mathbf{k}; \mathbf{q}) = \cos(k_x + 2q_x) - \cos(k_y + q_x + q_y) - \cos(k_y - q_x + q_y) + \cos(k_x + q_x + q_y) + \cos(k_x - q_x - q_y) - \cos(k_y + 2q_y) + \cos(k_x - q_x) + \cos(k_x - q_y) - \cos(k_y - q_x) - \cos(k_y - q_y) + \cos(k_x + q_y) - \cos(k_y + q_x)$, $\epsilon(\mathbf{k}; \mathbf{q}) = \frac{2}{k} \frac{2}{k+q} \epsilon(\mathbf{k}) + \frac{2}{k} \frac{2}{k+q} \epsilon(\mathbf{k} + \mathbf{q}) + 1$, $\epsilon(\mathbf{k}; \mathbf{q}) = \frac{2}{k} \frac{2}{k+q} \epsilon(\mathbf{k}) + \frac{2}{k} \frac{2}{k+q} \epsilon(\mathbf{k} + \mathbf{q}) + 1$, $G_k^0(\omega) = \frac{1}{\omega - E_k}$ is the bare Green's function, $E_k = \frac{1}{2} (k_x^2 + k_y^2) = \frac{1}{2} (k^2) = [1 + (\frac{1}{2}) (k^2)] = E_k/2$, and $k_0 k_1 = k = (2E_k)$.

It is noted that V_m is absent from Eq. (2) because there is no first order contribution from the magnetic potential. In the present study, we base our numerical calculation on a finite lattice of 800×800 lattice sites with the defect at the center. For simplicity, we choose $2t = V_s = 2t_1 = 4t_2$, and assume that all these parameters are small such that the first order T-matrix approximation is valid. The advantage of this first order approximation is that the states of quasiparticle before and after scattering from the defect are clearly distinguishable. In our calculation, we also introduce a finite lifetime broadening $\Gamma = 2$ meV to the quasiparticle

Green's function to smooth our data points by replacing $\omega - i0^+$ with $\omega - i$ in Eq.(2).

It is well-known that the quasiparticles in a d-wave superconductor are Bloch wave states. In the presence of electron-impurity interactions, elastic scattering mixes those eigenstates of the quasiparticle with the same energy but different momentum. For example, if a quasiparticle with energy E_k is excited at the point O in Fig. 1(a), after being scattered by the defect, the quasiparticle energy become E_{k+q} (E_k). There are 6 nonequivalent q vectors as shown in Fig. 1(a). The variation in the magnitudes of these q vectors with μ_0 would lead to energy-dependent LDOS modulations.

According to Eq. (2), we plot the image map of the Fourier component of LDOS in Fig. 1(b) for the optimally doped case at fixed $\mu_0 = 16$ meV in the first Brillouin zone. In Fig. 1(b) we are able to clearly identify four of the six q vectors as shown in Fig. 1(a) from the positions of the peaks (or local maxima). The four peaks with relatively weak intensity along $(\pm\pi; 0)$, $(0; \pm\pi)$ directions and the four peaks with relatively strong intensity along $(\pm\pi; \pm\pi)$ directions as shown in Fig. 1(b) are respectively related to q_A and q_B in Fig. 1(a), and both of them have been observed in Ref. [3]. In addition, we predict that there are another eight weak peaks corresponding to q_C . At the four corners of the first Brillouin zone, there are four extended weak peak arcs generated from the quasiparticle interference between the banana-shaped equal-energy contours of the diagonal Fermi surfaces connected by q_D . Since the peaks at q_B have the highest intensity, we expect that the real space LDOS image at $\mu_0 = 16$ meV should have a checkerboard pattern oriented along 45° to the Cu-O bonds with a period close to $5a$.

In Fig. 2(a) to 2(c), the q -space LDOS maps for the optimally doped case are also presented at $\mu_0 = 0$; 12; 20 (meV) in the first Brillouin zone. We noticed that the detailed image of the map depends on the magnitude of μ_0 , when it increases, j_A becomes shorter while j_B , j_C and j_D become longer. In Fig. 2(c) with $\mu_0 = 20$ meV, the intensity of the peaks at q_A is catching up with that at q_B as compared with the case of $\mu_0 = 16$ meV. And it is expected to become dominant at a larger μ_0 , there, the real space LDOS image would have a checkerboard pattern oriented along the Cu-O bonds with a period close to $4a$. This is consistent with the experiment in Ref. [3].

It needs to be mentioned that the peaks corresponding to the remaining two modulation wave vectors q_E and q_F [see Fig. 1(a)] are clearly missing in these maps [see Fig. 1(b), and Fig. 2(a) to 2(c)]. At $\mu_0 = 0$ meV, q_D and q_E are equivalent and a small arc peak is created at them, but the resolution of the map is not clear enough to show the existence of q_F (i.e. q_A and q_C). For $\mu_0 = 12$; 16; 20 (meV), both of these wave vectors do

not appear in the first Brillouin zone, but they may yield local peaks in the second Brillouin zone. So far the experiments have not yet been performed in this region, their effects will not be considered in the present study. But we do expect that the peaks associated with these wave vectors would show up when the boundary of our calculation is expanded beyond that of the first Brillouin zone. Here we would like to point out that although our images at $\mu = 12$ meV is similar to corresponding one in Ref. [3], there still exist some fundamental differences between these two results. For example, the bright spots (the dominant peaks) at points $(\pi; 0)$ appeared in the images of Ref. [3] close to $\mu = 20$ meV did not show up in our maps. If this prediction in Ref. [3] is true, the real space LDOS would have a checkerboard pattern with the period $1.414a$ oriented along 45° to the Cu-O bonds, which seems to be contradicting to the experimental observation [3].

At $\mu = 12; 16; 20$ (meV), the maps of the Fourier component of LDOS for the optimally doped case are shown in Fig. 2(d) to (f). The modulation wave vectors are identical to those for the negative μ . But the Fourier component of LDOS at q_B, q_C and q_D shows a local minimum intensity. This is primarily due to the destructive interference between the opposite phases carried by the quasiparticles before and after scattering. This destructive interference has also been observed at $\mu = 16; 22$ (meV) in the STM experiment of Ref. [3] (see Fig. 2C and 2D there). Obviously, the wave vectors at extreme (maximum or minimum) values of $q(\mu)$ for the positive μ coincide with those in Fig. 1(b), Fig. 2(b) and 2(c). In addition, we also found that in higher energy region close to the maximum of the superconductivity gap, our images become blurred. The reason is not clear to us, but it might be due to many competing modulation wave vectors gaining strengths on the same banana shaped equal energy contour of the Fermi surface.

In order to compare with the experimental curves in Ref. [3], Fig. 3 shows the Fourier component of LDOS respectively along $(\pi; 0)$ [Fig. 3(a)] and $(0; \pi)$ [Fig. 3(b)] directions as a function of q up to $q = 0.4$ (in unit of $2\pi/a$) for the optimally doped sample. Along $(\pi; 0)$ direction, the peak of $q(\mu)$ associated with q_A moves slowly towards the origin when energy increases. In contrast, along $(0; \pi)$ direction, the peak of $q(\mu)$ associated with q_B moves rapidly away from the origin. This energy-dependent position of the peaks at q_A or q_B is responsible for the checkerboard pattern with an energy-dependent period as observed in Ref. [3]. In the presence of other competing modulation wave vectors at higher energy, the LDOS image pattern could be dramatically modified.

We also study the effects of doping on $q(\mu)$. Fig. 4 shows the peak positions at q_A along $(\pi; 0)$ direction [Fig. 4(a)] and at q_B along $(0; \pi)$ direction [Fig. 4(b)] as a function of μ at three different dopings. As energy

is fixed, q_A becomes smaller while q_B becomes larger as the doping is increased. It is apparent that the results in Fig. 3 and 4 are in qualitative agreement with those experimental curves in Ref. [3].

In summary, we have studied the energy-dependent LDOS modulations in d-wave superconductors with the presence of an extended defect using the Bogoliubov transformation plus the Green's function approach. The changes in pairing order parameter and hopping terms due to such an extended defect generate some k and q dependent terms as shown in Eq. (2), which seem to be essential for obtaining the curves in Figs. 3 and 4. In addition, we also discover new modulation wave vectors q_C and q_D in the first Brillouin zone. Hopefully, their effects could be observed in future experiments. Since the effects of the modulation wave vectors in the second Brillouin zone have not been carefully examined, we are not able to obtain the complete LDOS image in real space. This is an important problem and should constitute a subject for future investigation. We also note that using the triangular relation $q_A + q_B = q_C$, the Fermi surface and the energy gap could be mapped out.

We wish to thank Prof. J. C. Davis for sending us Ref. [3] before its publication, and H. Y. Chen, M. Shaw, Y. Chen and Prof. S. H. Pan for useful discussions. This work has been supported by the Texas Center for Superconductivity at the University of Houston and by the Robert A. Welch Foundation.

-
- [1] J. E. Hoffman, E. W. Hudson, K. M. Lang, V. Madhavan, H. Eisaki, S. Uchida, J. C. Davis, *Science* 295, 466 (2002).
 - [2] C. Howald, H. Eisaki, N. Kaneko, A. Kapitulnik, *cond-mat/0201546*.
 - [3] J. E. Hoffman, K. McElroy, D.-H. Lee, K. M. Lang, H. Eisaki, S. Uchida, and J. C. Davis, *Science* 297, 1148 (2002).
 - [4] Y. Chen, H. Y. Chen, and C. S. Ting, *Phys. Rev.* 66, 104501 (2002).
 - [5] D. Podolsky, E. Demler, K. Damle, and B. I. Halperin, *cond-mat/0204011*.
 - [6] M. Vojta, *cond-mat/0204284*.
 - [7] Degang Zhang, *Submitted to Phys. Rev. B*.
 - [8] Qiang-Hua Wang and Dung-Hai Lee, *cond-mat/0205118*.
 - [9] J. H. Han, *cond-mat/0206284*.
 - [10] A. Polkovnikov, S. Sachdev, and M. Vojta, *cond-mat/0208334*.
 - [11] M. R. Norman, M. Randeria, H. Ding, and J. C. Cam-puzano, *Phys. Rev. B* 52, 615 (1994).
 - [12] Jian-Ming Tang and M. E. Flatte, *Phys. Rev. B* 66, 060504 (2002).

FIG. 1. (a) Schematic Fermi surface of high- T_c cuprate superconductor. The modulation wave vectors connecting different points of the Fermi surface with the same energy gap are shown. (b) The Fourier component of LDOS $\rho_q(\epsilon)$ for the optimally doped case at $\epsilon = 16$ meV in the first Brillouin zone (i.e. $-\pi < q_x, q_y < \pi$).

FIG. 2. The Fourier component of LDOS $\rho_q(\epsilon)$ for the optimally doped case at different energy shown in each panel in the first Brillouin zone.

FIG. 3. $\rho_q(\epsilon)$ versus q_x, q_y for the optimally doped case along (a) the $(\pi; 0)$ direction and (b) the $(\pi; \pi)$ direction are shown for seven quasiparticle energies. The data are shifted vertically relative to each other by 0.5 unit for clarity.

FIG. 4. The modulation wave vectors versus energy along (a) the $(\pi; 0)$ direction and (b) the $(\pi; \pi)$ direction are plotted for under-, optimally and over-doped cases.

Fig. 1 Zhang and Ting

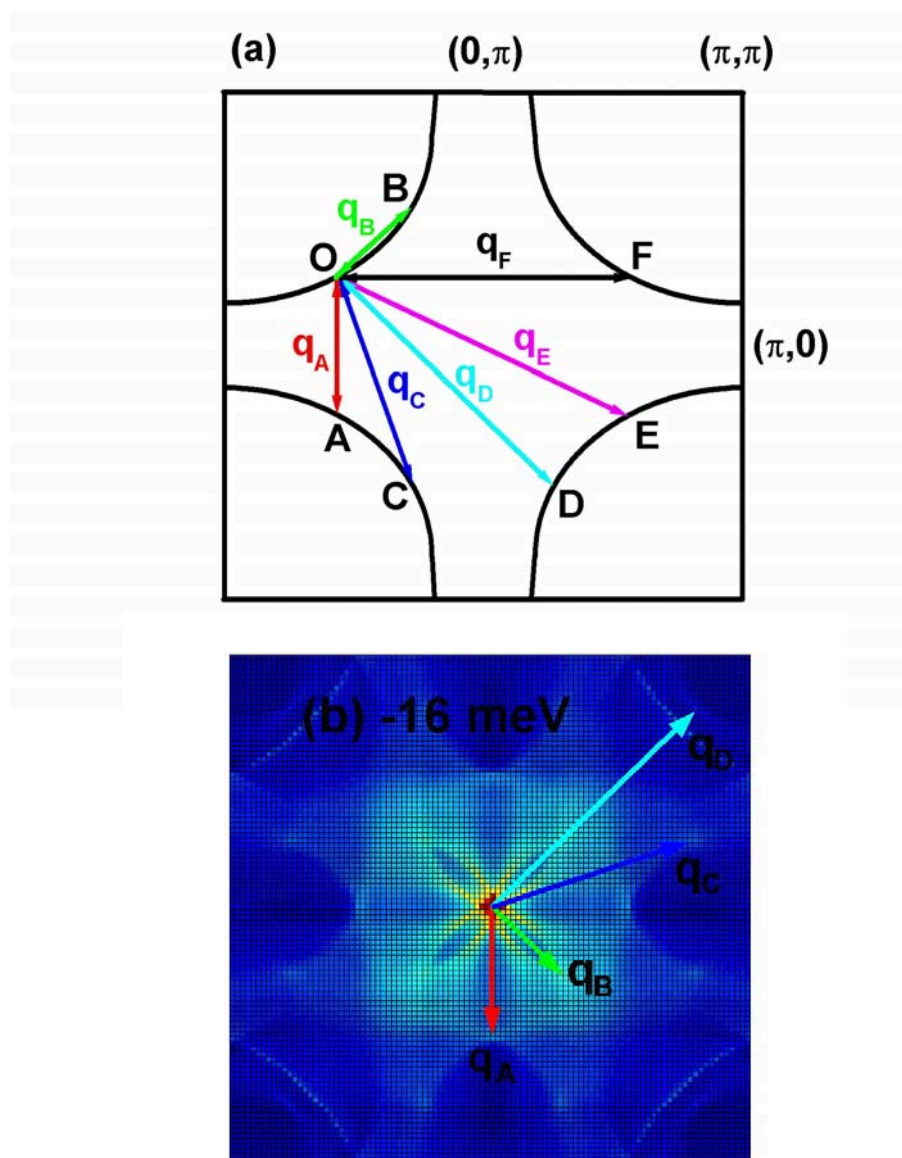


Fig. 2 Zhang and Ting

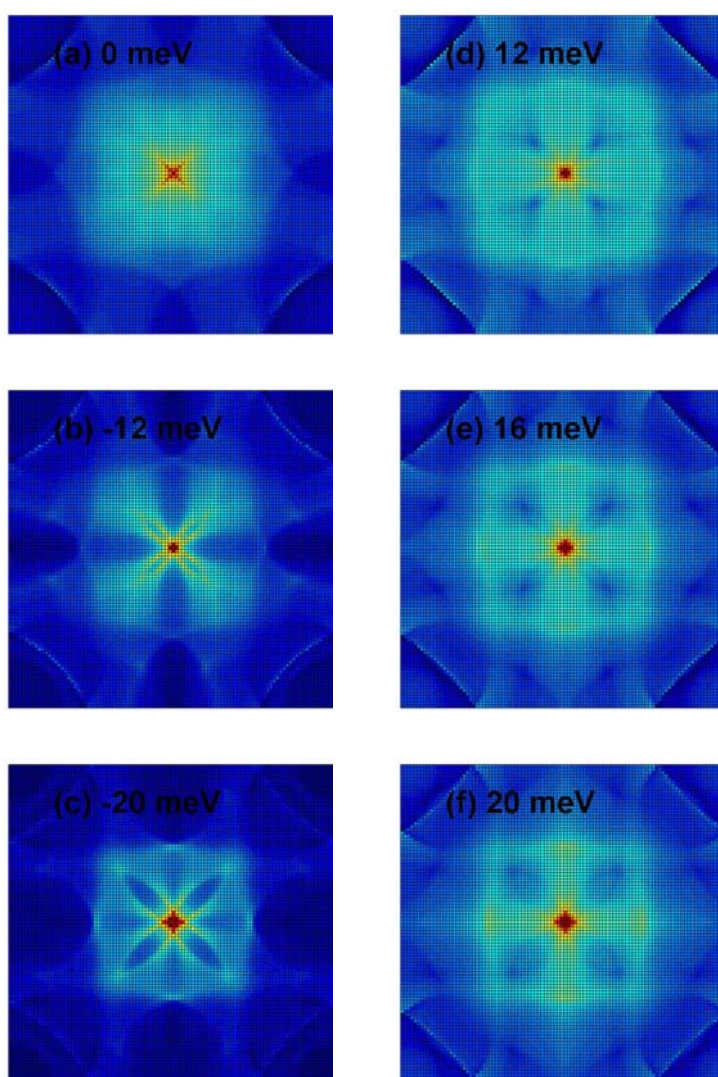


Fig. 3 Zhang and Ting

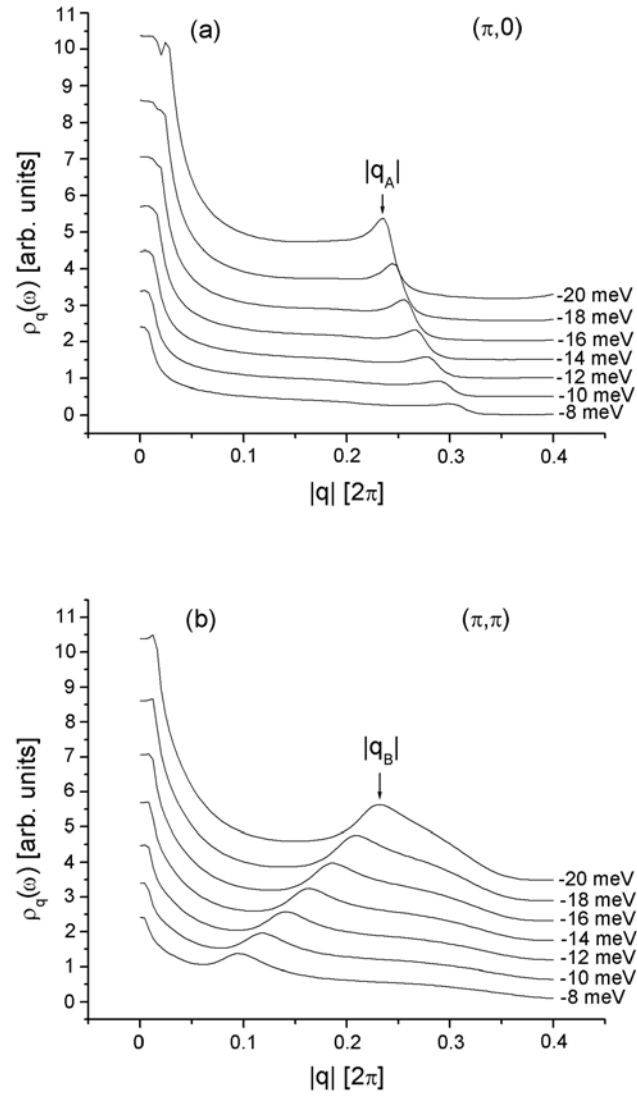


Fig. 4 Zhang and Ting

